

Characterization of New-Generation Silicon Photomultipliers for Nuclear Security Applications

Marc A. Wonders, David L. Chichester, *Senior Member, IEEE*, and Marek Flaska, *Member, IEEE*

Abstract— Silicon photomultipliers have received a great deal of interest recently for use in applications spanning a wide variety of fields, including nuclear safeguards and nonproliferation. For nuclear-related applications, the ability of silicon photomultipliers to discriminate neutrons from gamma rays using pulse shape discrimination when coupled with certain organic scintillators is a characteristic of utmost importance. This work reports on progress characterizing the performance of twenty different silicon photomultipliers from five manufacturers with an emphasis on pulse shape discrimination performance and timing. Results are presented on pulse shape discrimination performance as a function of overvoltage for 6-mm x 6-mm silicon photomultipliers, and the time response to stilbene is characterized for silicon photomultipliers of three different sizes. Finally, comparison with a photomultiplier tube shows that some new-generation silicon photomultipliers can perform as well as photomultiplier tubes in neutron-gamma ray discrimination.

I. INTRODUCTION

THE ability to detect neutrons and characterize their sources is essential for a variety of nuclear security and safeguards tasks. For decades, the standard method of doing so has been the use of ^3He proportional counters, but an increase in its demand coupled with a decrease in production has created a push for the development of alternative methods of detecting neutrons [1]. A promising candidate to replace ^3He detectors is the scintillation detector. Organic scintillators are capable of detecting fast neutrons, and neutron capture agents such as ^6Li enable the detection of thermal neutrons when incorporated in some scintillating media [2].

All scintillation detectors require some means of converting the optical signal into an electrical signal and amplifying this signal to a measurable amount. A photomultiplier tube (PMT) has been the traditional tool used for this purpose because of its high gain, low noise, and fast response. However, applications requiring low level light sensing in alternate packaging and with other features have stimulated the development of alternative light sensors. A silicon

photomultiplier is one such recent development. Silicon photomultiplier devices are called many different names based on the manufacturer, including Geiger-mode avalanche photodiode, multi-pixel photon counter, and solid state photomultiplier, but in this work all these devices will be referred to as silicon photomultipliers (SiPMs). SiPMs are an evolution of the avalanche photodiode and are essentially many avalanche photodiodes miniaturized and connected in parallel [3]. Each avalanche photodiode is generally connected in series with a quenching resistor and this combination of avalanche photodiode and quenching resistor constitutes a microcell of the SiPM.

By operating these avalanche photodiodes in Geiger mode high gain is achieved, and the presence of many different microcells enables signal proportionality. SiPMs have been shown to have excellent time and energy resolution, and comparable gain to many PMTs. They also offer additional advantages characteristic of solid state technology such as mechanical ruggedness, insensitivity to magnetic fields, compactness, and a much lower operating voltage than PMTs [4].

Their main drawback has been higher noise levels than PMTs which is primarily caused by thermal generation of charge carriers in the avalanche region of the SiPM that produce a signal indistinguishable from optically produced charge carriers. Improved performance at low temperatures has consequently been shown, but recent improvements in SiPM technology have also made effective operation at room temperature feasible [4]. Thus, SiPMs are drawing interest in fields as diverse as medical physics, high energy physics, and homeland security. This paper focuses on applications to homeland security and, as such, reports on progress in characterization of a suite of different SiPMs in regard to their ability to discriminate neutrons from gamma rays when coupled to an organic scintillator, as well as their timing properties.

II. SiPMs AND EXPERIMENTAL SETUP

For this work SiPMs were acquired from five different manufacturers: AdvanSiD, First Sensor, Hamamatsu, Ketek, and SensL [5-9]. Of the packages available from each company, packages were selected that provided direct access to the anode and cathode via conducting pins. These were chosen to both minimize any pulse shaping via added built-in circuitry and provide as uniform testing conditions as possible. The SiPM sizes are 3 mm x 3 mm, 4 mm x 4 mm, and 6 mm x

This material is based upon work supported by the US Department of Energy's National Nuclear Security Administration Office of International Nuclear Safeguards, from the Human Capital Development Subprogram.

M. A. Wonders and M. Flaska are with the Department of Mechanical and Nuclear Engineering, Pennsylvania State University, University Park, PA 16802-4400 (e-mail: mfw5173@psu.edu, mflaska@psu.edu)

D. L. Chichester is with Idaho National Laboratory, Idaho Falls, ID 83402 (e-mail: david.chichester@inl.gov)

6 mm, and microcell sizes range from 15 μm to 75 μm . Only one package was selected from each manufacturer except SensL, from which two different package forms were acquired. Only SensL and Ketek provided two different SiPM series; the full list of SiPMs acquired are shown below in Table I. The SiPMs themselves are shown in Fig. 1.

TABLE I
CHARACTERISTICS OF SiPMs ACQUIRED

Manufacturer	Pixel Size (mm)	Microcell Size (μm)	Series	Package	Typical Breakdown Voltage (V)
AdvanSiD	3	40	ASD-NUV	Socket	26
AdvanSiD	4	40	ASD-NUV	Socket	26
First Sensor	3	40	NUV	SMD	26
First Sensor	4	40	NUV	SMD	26
Hamamatsu	3	25	S13360	Cs	53
Hamamatsu	3	50	S13360	Cs	53
Hamamatsu	3	75	S13360	Cs	53
Hamamatsu	6	25	S13360	Cs	53
Hamamatsu	6	50	S13360	Cs	53
Hamamatsu	6	75	S13360	Cs	53
Ketek	3	15	WB	PM	27.5
Ketek	3	25	WB	PM	27.5
Ketek	6	25	EB	PM	26.5
Ketek	6	50	EB	PM	26.5
SensL	3	20	C	SMTPA	24.5
SensL	3	35	C	SMTPA	24.5
SensL	3	35	J	SMTPA	24.5
SensL	3	50	C	SMTPA	24.5
SensL	3	35	C	X13	24.5
SensL	6	35	C	X13	24.5

It should be noted that all the SiPMs studied here have breakdown voltages around 25 V except the Hamamatsu SiPMs, which have breakdown voltages around 53 V. This will have consequences when looking at characteristics based on overvoltage in which the fraction of breakdown voltage will provide more similar results than absolute magnitude of the overvoltage.

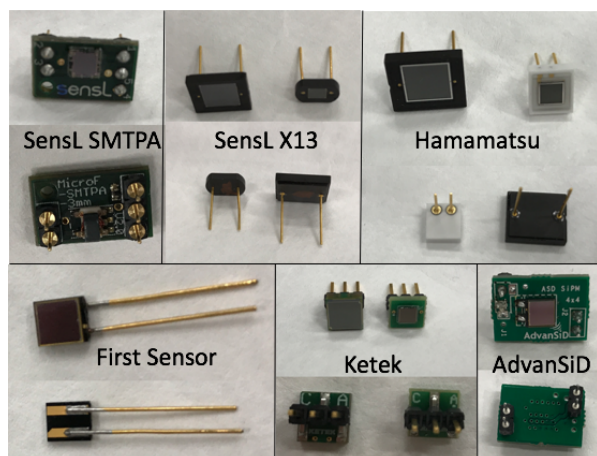


Fig. 1. The SiPMs used in this study.

As seen in Fig. 1, despite all SiPMs having similar readouts, the pins themselves are oriented differently, complicating somewhat the uniform setup of all SiPMs. For this reason, the

SiPMs were setup using a simple breadboard with a typical wire layout used to interface with the breadboard as shown in Fig. 2. Measurements were conducted in a light-tight box to minimize wrapping requirements for the scintillator and SiPM combination. The trace from the SiPM was digitized using a 14-bit CAEN DT5730 digitizer with a sampling rate of 500 GHz and analyzed offline using the ROOT data analysis framework [10].

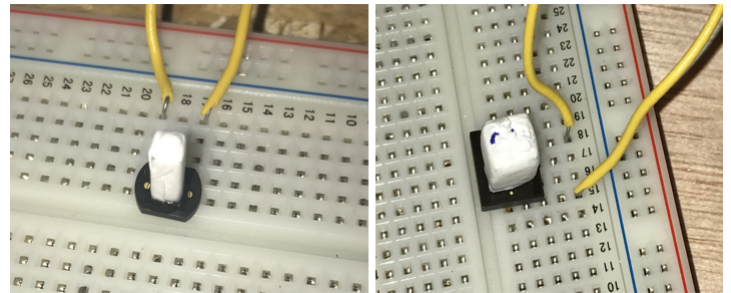


Fig. 2. Biasing and signal readout setup.

Stilbene was chosen as the scintillator for this work because of its excellent ability to perform pulse shape discrimination (PSD). Two different sizes were used: a 3-mm x 3-mm x 10-mm crystal for the 3-mm x 3-mm and 4-mm x 4-mm SiPMs and a 6-mm x 6-mm x 6-mm crystal with the 6-mm x 6-mm SiPMs. The crystals used are shown in Fig. 3. The maximum photon detection efficiencies for the SiPMs used in this study range from 420 nm to 450 nm, yielding effective though imperfect matching of stilbene's emission spectrum, which peaks around 380 nm. The crystals were wrapped in reflective Teflon tape and coupled to the SiPMs using EJ-550 optical grease from Eljen Technology to maximize light collection by the SiPMs [11]. The Teflon wrapping was not changed during these tests.



Fig. 3. The stilbene crystals used in this study.

III. WAVEFORMS

To visualize and quantify the different timing properties of the SiPMs, a ^{137}Cs gamma ray source was used to irradiate the stilbene scintillators. Because stilbene has a very fast decay time on the order of nanoseconds, the different pulse widths observed for each SiPM are largely representative of the SiPM itself and close to the microcell response time for each.

One-hundred pulses from each SiPM were averaged together and then normalized, and these are shown in Figs. 4-7. The full-width tenth-max was determined for each measurement by taking the mean of a Gaussian distribution fit to the distribution of full-width tenth-max values determined over roughly one-hundred thousand events. The rise time of each SiPM was determined in the same manner, where the rise time was calculated as the time between the last sample below 10% of the pulse height and the sample of maximum pulse height. These values are shown in Table II.

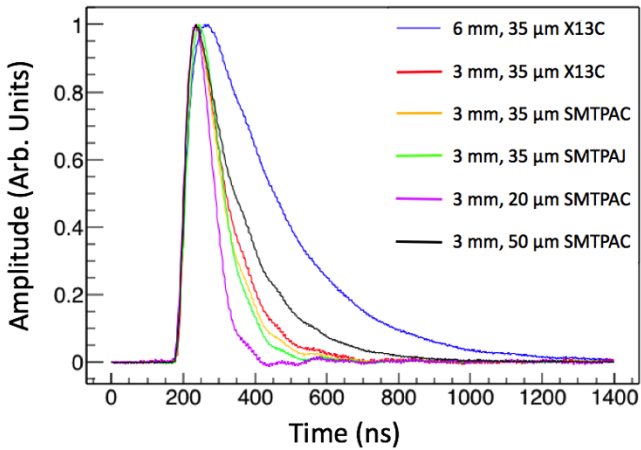


Fig. 4. SensL waveforms.

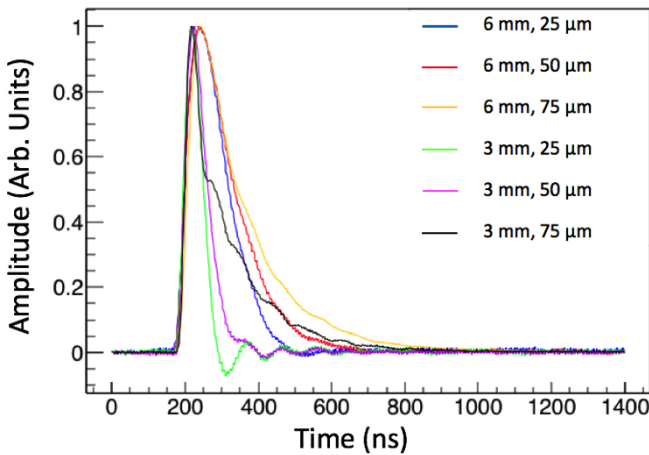


Fig. 5. Hamamatsu waveforms.

From Figs. 4-7 a wide variety of pulse widths are observed ranging from about 100 ns to 600 ns. As expected, larger SiPMs tend to have longer pulses because of their larger capacitances, and it is also observed that for a given SiPM size larger microcells tend to have longer pulses. Despite large differences in pulse width, all SiPMs tested have similar rise times. The undershooting seen in the fastest SiPMs can be removed by adding a small resistance in series after the output of the SiPM but was not included in the setup used here, in order to show unaltered pulse widths for all the devices and provide uniform signal processing for all.

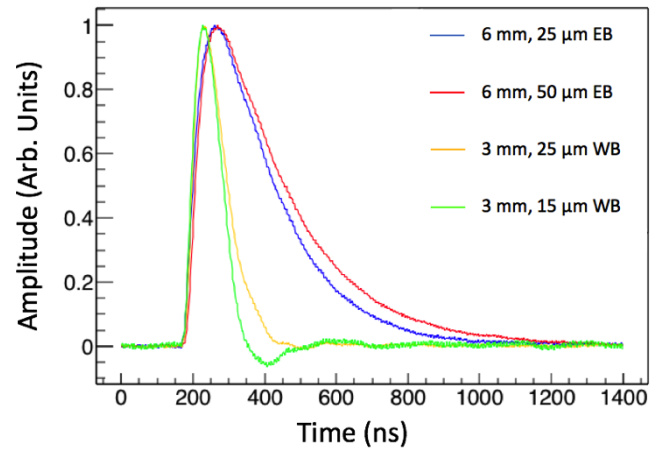


Fig. 6. Ketek waveforms.

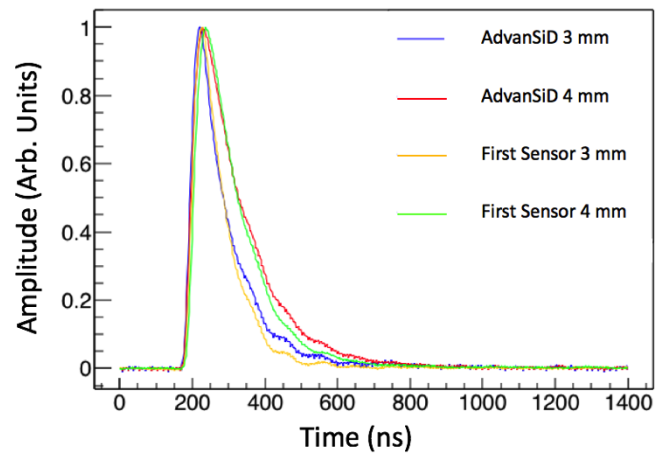


Fig. 7. AdvanSiD and First Sensor waveforms.

TABLE II
TIMING CHARACTERISTICS OF SiPMs TESTED

Manufacturer (Series, Package)	Pixel Size (mm)	Microcell Size (μm)	Rise Time (ns)	Full-Width Tenth-Max (ns)
AdvanSiD	3	40	22.6	240.2
AdvanSiD	4	40	26.4	325.4
First Sensor	3	40	22.6	221.4
First Sensor	4	40	25.8	317
Hamamatsu	3	25	23	94.4
Hamamatsu	3	50	22.2	138.4
Hamamatsu	3	75	20.2	250.6
Hamamatsu	6	25	27	227.6
Hamamatsu	6	50	27	293.8
Hamamatsu	6	75	26.4	358.2
Ketek (WB)	3	15	26.2	139
Ketek (WB)	3	25	25.2	191.2
Ketek (EB)	6	25	27.4	501
Ketek (EB)	6	50	27.6	591
SensL (C, SMTPA)	3	20	25.6	167
SensL (C, SMTPA)	3	35	25.8	250
SensL (C, SMTPA)	3	50	26	372
SensL (J, SMTPA)	3	35	27.4	229.6
SensL (C, X13)	3	35	26.4	276.2
SensL (C, X13)	6	35	27.4	605.8

For manufacturers that provided more than one package or series, this information is also specified in Table II.

IV. PULSE SHAPE DISCRIMINATION PERFORMANCE

A primary motivating factor for the assessment of SiPMs for nuclear security is their application to neutron detectors, especially organic scintillators that are sensitive to both gamma rays and neutrons. Sensitivity to gamma rays of organic scintillators is generally overcome by analyzing the temporal profiles of pulses using the popular technique of PSD. Because neutrons primarily interact with protons while gamma rays primarily interact with electrons, neutron interactions produce charged particles with higher specific ionization [12]. This creates a higher concentration of triplet states in the scintillator, which enables more frequent triplet-triplet annihilations to occur after the initial light production and, consequently, produces a greater amount of delayed scintillation light. Many ways of exploiting differences in the pulse shape exist to discriminate neutrons and gamma rays including charge comparison, pulse gradient analysis, and frequency gradient analysis [13]. Charge comparison is the most frequently used method because of its effectiveness and simplicity of implementation and is the focus of this paper. In this method, a tail integral and total integral are defined and the ratio of these two values is a pulse shape parameter (PSP) that provides a measure of the amount of delayed light that identifies neutrons and gamma rays. Example neutron and gamma ray pulses are shown in Fig. 8.

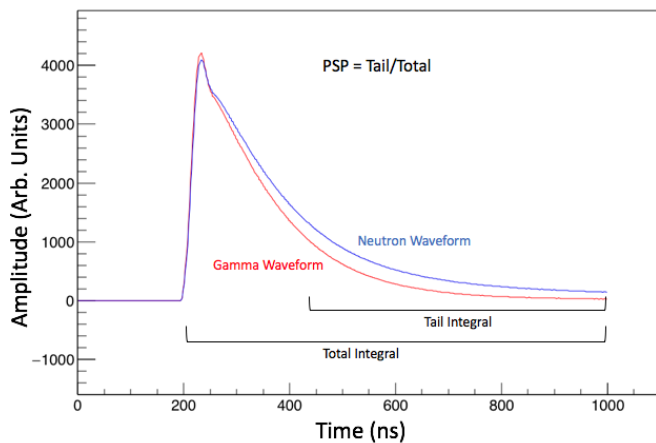


Fig. 8. Depiction of the charge comparison method for neutrons and gamma rays.

A typical one-dimensional histogram of the pulse shape parameter is shown in Fig. 9. The grouping at larger values of the pulse shape parameter corresponds to neutrons. To quantify the effectiveness of PSD between neutrons and gamma rays, Gaussian shapes are fit to each distribution and used to create a figure of merit (FOM, defined in Equation 1).

$$FOM = \frac{\text{Distance Between Peaks}}{FWHM_N + FWHM_G} \quad (1)$$

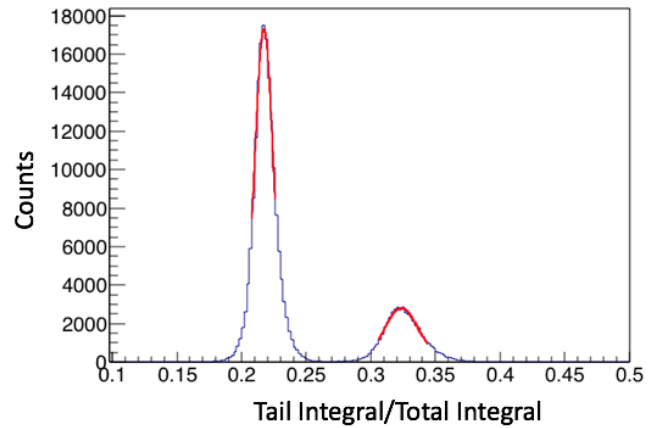


Fig. 9. Example PSD histogram (blue) with Gaussian fits (red) to each distribution.

As seen in Figs. 4-7, the 3-mm x 3-mm and 4-mm x 4-mm SiPMs exhibit undershooting and ringing, and this likely deteriorates the PSD that would be present with an ideal readout. The 6-mm x 6-mm in the setup used produce much smoother pulses optimized for PSD performance likely because of their slower rising edge. Consequently, PSD results will only be shown for the 6-mm x 6-mm SiPMs.

For each SiPM the FOM is determined in the light output window between 200 and 1000 keVee. Calibration is performed using the Compton edge of ¹³⁷Cs. The PSD performance as a function of overvoltage for the 6-mm x 6-mm SiPMs is shown in Fig. 10.

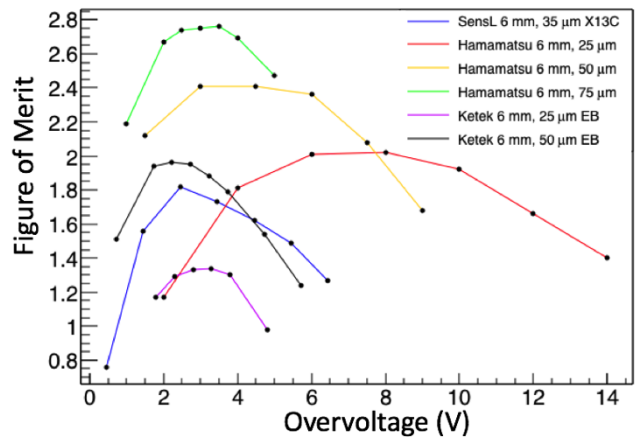


Fig. 10: Pulse shape discrimination performance as a function of overvoltage for 6-mm x 6-mm SiPMs.

All SiPMs initially exhibit improved PSD performance with increasing overvoltage and then reach a plateau with the optimum PSD before the PSD deteriorates. The decrease in PSD performance as overvoltage approaches 0 V is driven at least partly by the presence of digitizer noise that limits the signal-to-noise ratio for smaller pulses. The plateaus occur generally around an overvoltage of 3 V, and it should be recalled that the breakdown voltage of Hamamatsu SiPMs is roughly twice that of the Ketek and SensL SiPMs, explaining the lengthening of and shift to higher overvoltages of their plateaus. Further, there is a greater range of microcell sizes

covered by Hamamatsu explaining the larger differences in plateau behavior within that manufacturer’s SiPMs. Table III displays the best FOM for each 6-mm x 6-mm SiPM.

TABLE III
PULSE SHAPE DISCRIMINATION PERFORMANCE OF 6-MM X 6-MM SiPMs

Manufacturer (Series, Package)	Microcell Size (μm)	Best Overvoltage (V)	Figure of Merit
Hamamatsu	75	3.5	2.76
Hamamatsu	50	3, 4.5	2.41
Hamamatsu	25	8	2.02
Ketek (EB)	50	2.73	1.96
SensL (C, X13)	35	2.45	1.82
Ketek (EB)	25	2.8	1.34

Table III is ordered by the FOM and there appears to be a correlation between FOM and microcell size. This relationship is shown explicitly in Fig. 11. The impact of the pulse width on the FOM is shown in Fig. 12, and no dependency is observed.

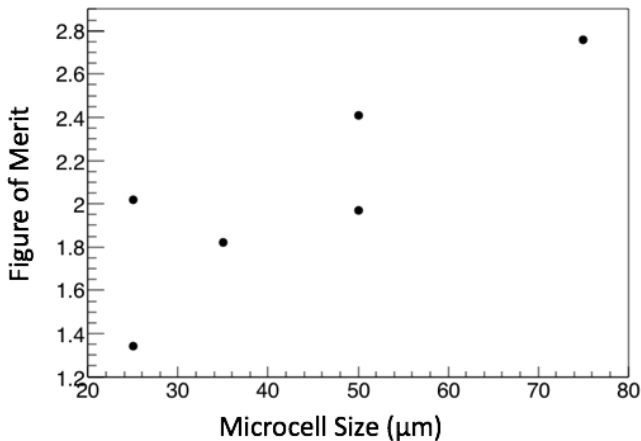


Fig. 11: Relationship between microcell size and FOM for 6-mm x 6-mm SiPMs.

A comparison of the PSD performance of these SiPMs with a fast PMT was also conducted. The 6-mm x 6-mm stilbene crystal was coupled to a Hamamatsu H10580 PMT assembly, and the FOM was calculated to be 1.88 in the 200-1000 keVee window and 2.31 in the 200-300 keVee window. The setup used for these tests is shown in Fig. 13, and the associated PSD plot is shown in Fig. 14. The PSD plot from the SiPM with the highest FOM is shown in Fig. 15.

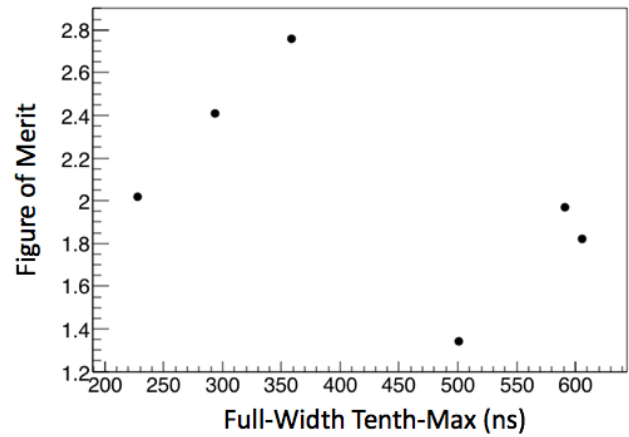


Fig. 12: Relationship between pulse width and FOM for 6-mm x 6-mm SiPMs.



Fig. 13: A 6 mm x 6 mm stilbene crystal coupled to a Hamamatsu H10580 PMT assembly.

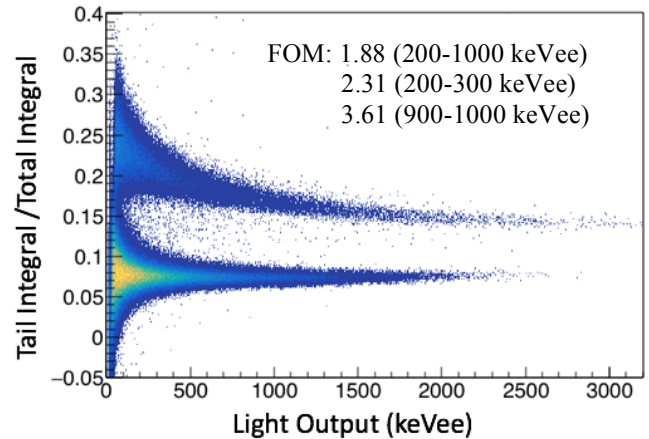


Fig. 14: Pulse shape discrimination plot for the H10580 PMT coupled to stilbene.

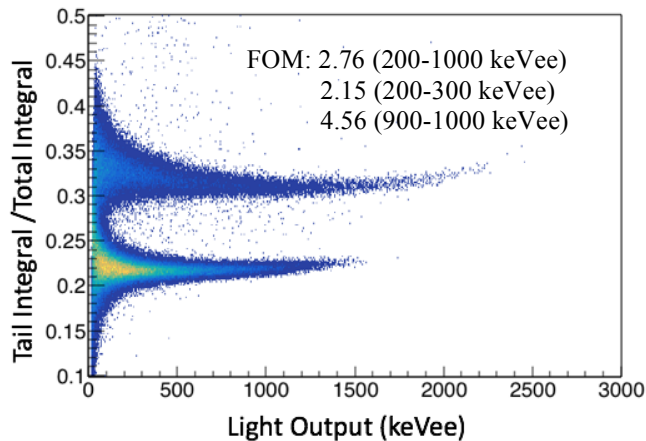


Fig. 15: Pulse shape discrimination plot for the S13360-6075CS SiPM coupled to stilbene.

V. CONCLUSIONS

The comparison between a fast PMT capable of effective PSD with SiPMs has shown that new generation SiPMs can perform competitively with PMT technology when coupled with organic scintillators. In terms of effective neutron detection and discrimination, results presented in this paper suggest that SiPMs with the largest microcells tend to perform better. The greater photon detection efficiency caused by a greater geometrical fill factor and the larger gain, defined as the charge produced from a single triggered charge avalanche, likely play a large role in this. As expected, all the SiPMs tested here had similar rise times despite large differences in overall pulse width, and no direct relationship between pulse width and PSD performance was observed between different SiPMs. PSD performance as a function of overvoltage eventually diminishes and this is likely a combination of a sharply increasing noise past a certain overvoltage and other factors such as saturation of the SiPM microcells. Further, the behavior of the PSD plateaus was seen to be affected significantly by the microcell size with smaller microcells showing peak PSD performance at higher overvoltages and over a greater range of overvoltages.

VI. FUTURE WORK

In addition to PSD results for the 6-mm x 6-mm SiPMs, only temporal profiles of the SiPMs have been presented here, and, as such, investigation into both noise and signal-to-noise ratios, where signal magnitude is proportional to both the gain and photon detection efficiency, are being carried out as complementary to the PSD results. Further, optimization of SiPM readout for smaller SiPMs will take place so that their PSD performance can be effectively characterized and compared to other SiPMs. This will provide greater support for relationships between different SiPM characteristics and PSD performance. Investigation into the effects of SiPM dynamic range and saturation of the microcells is also necessary, and the acquisition of a picosecond light pulser will allow for tests of wavelength sensitivity and timing response to ultrafast light pulses. Finally, testing of the effects of elevated temperature and radiation damage on the SiPMs will be conducted.

REFERENCES

- [1] A.P. Simpson, et al., "A review of neutron detection technology alternatives to helium-3 for safeguards applications," *INMM 52nd Annual Meeting*, vol. 8, 2011.
- [2] P. Peerani, et al., "Testing on novel neutron detectors as alternatives to ^3He for security applications," *Nucl. Instr. and Meth. A*, vol. 696, pp. 110-120, Dec. 2012.
- [3] P. Buzhan, et al., "Silicon photomultiplier and its possible applications," *Nucl. Instr. and Meth. A* vol. 504, no. 1-3, pp. 48-52, May 2003.
- [4] P. K. Lightfoot, "Characterisation of a silicon photomultiplier device for applications in liquid argon based neutrino physics and dark matter searches," *Journal of Instrumentation*, vol. 3, Oct. 2008.
- [5] AdvanSiD, Trento, Italy
- [6] First Sensor, Berlin, Germany
- [7] Hamamatsu, Shizuoka Prefecture, Japan
- [8] Ketek, Munich, Germany
- [9] SensL, Cork, Ireland
- [10] R. Brun and F. Rademakers, "ROOT – An object oriented data analysis framework," *Nucl. Instr. and Meth. A.*, vol. 389, no. 1-2, pp. 81-86, Apr. 1997.
- [11] Eljen, Sweetwater, Texas, United States of America
- [12] M. L. Roush, "Pulse shape discrimination," *Nuclear Instruments and Methods*, vol. 31, no.1, pp. 112-124, Dec. 1964.
- [13] C. Liao and H. Yang, "Pulse shape discrimination using EJ-299-33 plastic scintillator coupled with a Silicon Photomultiplier array," *Nucl. Instr. and Meth. A.*, vol. 789, pp. 150-157, Jul. 2015.